Available online at www.sciencedirect.com
ScienceDirect
International Journal of Heat and Mass Transfer 51 (2008) 1192–1204
International Journal of HEAT and MASS TRANSFER
www.elsevier.com/locate/ijhmt

Two-phase flow modeling of liquid-feed direct methanol fuel cell

T.Z. Yan, Tien-Chien Jen *

Mechanical Engineering Department, University of Wisconsin at Milwaukee, Milwaukee, WI 53211, United States

Received 17 September 2006; received in revised form 7 March 2007
Available online 23 May 2007

Abstract

A two-phase flow model was developed for liquid-feed methanol fuel cells (DMFC) to evaluate the effects of various operating parameters on the DMFC performance. In this study, a general homogenous two-dimensional model is described in details for both porous layers and fluid channels. This two-dimensional general model accounts for fluid flow, electrochemical kinetics, current density distribution, hydrodynamics, multi-component transport, and methanol crossover. It starts from basic transport equations including mass conservation, momentum transport, energy balance, and species concentration conservation in different elements of the fuel cell sandwich, as well as the equations for the phase potential in the membrane and the catalyst layers. These governing equations are coupled with chemical reaction kinetics by introducing various source terms. It is found that all these equations are in a very similar form except the source terms. Based on this observation, all the governing equations can be solved using the same numerical formulation in the single domain without prescribing the boundary conditions at the various interfaces between the different elements of the fuel cell. The numerical simulation results, such as velocity field, local current density distribution, and species concentration variation along the flow channel, under various operation conditions are computed. The performance of the DMFC affected by various parameters such as temperature, pressure, and methanol concentration is investigated in this paper. The numerical results are further validated with available experimental data from the published literatures.

Keywords: Direct methanol fuel cell; DMFC; Two-phase flow model

1. Introduction

Direct methanol fuel cells (DMFCs) using polymer electrolyte membrane (PEM), have demonstrated improved performance and received increased attention [1,2]. Compared with conventional proton exchange membrane fuel cells (PEMFCs) (using H_2), DMFCs have the following advantages; easy fuel delivery and storage, no need for cooling or humidification, and simpler system design [3]. And they may even achieve higher overall energy efficiency than PEMFCs with further development [4].

Currently, two types of DMFC have been developed. In one of them methanol is supplied to the anode under elevated temperature (typically 110–130 °C) in gaseous form. The other type of cell works at low temperature (typically 80 °C) with liquid methanol as fuel. Both types have advantages and disadvantages. Methanol ionization proceeds better in the high temperature cell. At high current densities, however, this cell suffers from membrane drying, which leads to degradation in cell performance. The low temperature cell exhibits lower electrochemical activity, but is fully hydrated and hence has no limitations related to membrane drying.

Although DMFC technology is quite promising, two technological obstacles still hinder its wider application, they are: low electro-activity of methanol oxidation on the anode, and substantial methanol crossover (“chemical short”) through the polymer membrane from the anode to cathode. Much work has focused on the two above-mentioned problems. Many researches tried to develop more active methanol electro-oxidation catalysts [5,6] and improve understanding of the methanol electro-oxidation mechanism [7], including studies on well-defined catalyst

* Corresponding author. Tel.: +1 414 229 2307; fax: +1 414 229 6958.
E-mail address: jent@uwm.edu (T.-C. Jen).

0017-9310/$ - see front matter © 2007 Published by Elsevier Ltd.
doi:10.1016/j.ijheatmasstransfer.2007.03.007

Nomenclature

a	vapor activity
C^{k}	the mass fraction of species k
$C_{\mathrm{ref}}^{\mathrm{MeOH}}$ and $C_{\mathrm{ref}}^{\mathrm{O_2}}$	reference concentration of MeOH and oxygen
c_0	the reference concentration
D	diffusivity
E_{cell}	the difference between the half-cell potentials of the anode and cathode, at the reference current density i_0
F	Faraday's constant
I	cell current density
I_{e}	ionic current density in membrane
I_{p}	parasitic current density
$i(z)$	local current density at the location z
i_0	the exchange current density at the reference concentration
$i_{\mathrm{a,ref}}^0$ and $i_{\mathrm{c,ref}}^0$	reference exchange current density at anode and cathode catalyst layer
j_{MeOH}	the flux of methanol crossover through the membrane
K	permeability, cm^2
M	the molecular weight of the fluid
M^k	the molecular weight of species k
$\dot{m}^k$	source/sink term for species equations
n	the number of electrons involved in the reaction
n_{d}^k	drag coefficient of species k in porous media
n_{Ri}	net electrode output of electrode reaction Ri
n_{drag}	drag factor
n_{d}	the fluid drag coefficient
p	pressure, Pa
p_{c}	the capillary pressure, Pa
R	gas constant
Re	Reynolds number
s	the liquid saturation
S_{Ri}^k	stoichiometric coefficient of species k in reaction Ri
S_u, S_v	source terms for u and v momentum equations
T	temperature, K
t_{m}	the membrane thickness
t_{l} and t_{g}	tortuosity for liquid and gas phase, respectively
U	Internal energy
u, v	velocity in x, y-direction
x^k	the molar friction of species k

Greek symbols

α_{a} and α_{c}	anodic and cathodic transfer coefficients
β	a constant related to the Tafel slope
ε	porosity
ε_{m}	membrane porosity
γ	the surface area per unit volume of the electrode
γ_α	advection correction factor
η_{a}	overpotential at anode
η_{c}	overpotential at cathode
η_{ohmic}	Ohmic overpotential
η_{crover}	the crossover overpotential
σ	protonic resistivity within the electrode
σ_{m}	ionic conductivity, mho/cm
ρ	density, $\mathrm{g/cm}^3$
Φ	cell potential, J/mol K
ν	kinematical viscosity, cm^2/s
μ	dynamic viscosity, g/cm s
κ_{rl}	relative permeability for liquid phase
κ_{rg}	relative permeability for gas phase
ν_{l}	kinetic viscosity for liquid phase
ν_{g}	kinetic viscosity for gas phase
λ_{l} and λ_{g}	relative mobilities for liquid and gas phases, respectively
χ	an empirical constant for methanol crossover through membrane

Subscripts

a	anode
avg	average
c	cathode
i	inlet condition
k	kth component
m	membrane
w	water

surface [8]. Basically, enhancing the catalyst activity can alleviate methanol crossover by operating DMFC in an optimal manner such that all methanol will be consumed at the anode catalyst layer before reaching the membrane. Different anode catalyst structures and composition such as Pt, Pt–Ru, etc. have been developed [9] and several different anode catalysts, such as, Pt and Pt–Ru have been explored [10–12]. In addition, the effects of the anode electrochemical reaction on fuel cell performance have been studied experimentally [8,10]. Some other attempts have been made to investigate the fundamental electrochemical reaction mechanisms, such as water, methanol, as well as gas management, flow field design and optimization. In particular, carbon dioxide evolution in the liquid-feed anode results in strongly two-phase flow condition, making the mechanisms of reactant supply and product removal more complicated. All these processes are intimately coupled, resulting in the existence of optimal cell design and operating conditions. A good understanding of this complex, interacting phenomena is thus essential and can be most likely achieved through a combined mathematical modeling and comprehensive experimental approach.

The early efforts of mathematical modeling are fairly simple, such as Verbrugge's diffusion model [13], Fuller's concentrated solution theory model and Scott's simplified 1-D model [14] for vapor-feed and liquid-feed DMFC. Especially, the methanol crossover was first considered in Scott's simplified model. An empirical expression was employed to determine the effect of methanol crossover on the cell voltage. This simplified 1-D model provided a basic understanding of the transport phenomena in DMFC. However, they treated the pores of electrode as if they are filled with solid polymer electrolyte, eliminating any void volume for the feed to occupy.

Later, Baxter et al. [15] developed a one-dimensional mathematical model for a liquid-feed DMFC, mainly focused on the anode catalyst layer and the effect of the electro-osmotic drag of water, which was derived from the friction coefficient of water and hydrogen ions. Mass transfer in the anode is defined in terms of a pseudo-mass-transport coefficient. And the anode reaction is modeled with the Butler–Volmer expression rather than Tafel kinetics, which is less accurate at low current densities. The methanol crossover was not considered in this model. Thus this model is limited to low methanol concentration behavior. At high methanol concentration, methanol crossover has significant affect on fuel cell performance; this model is unable to give accurate prediction.

Wang and Savinell [16] developed a 1-D macro-homogeneous model to describe the reaction and transport within the catalyst zone of the methanol electrode. In their study, they neglected the effect of the diffusion layer due to the current density is not very high. They investigated the effects of the anode catalyst thickness, catalyst loading and polymer electrolyte loading on cell performance. Their results show that methanol crossover has a strong correlation with the catalyst utilization. It also shows that the correlation of the catalyst utilization and the methanol crossover is dependent on the rate of ionic resistance and mass transport resistance. Dohle et al. [17] presented a 1-D model for the vapor-feed DMFC and the crossover phenomenon was described. The effects of methanol concentration on the cell performance were studied.

All these models are one-dimensional: it is assumed that the cell is uniform in the lateral direction and the transport kinetic processes vary only across the cell. There are, therefore, two sources of two-dimensional effects: non-uniform distributions of species concentration and non-uniform electric potential in the carbon phase along the flow direction. Due to these reasons, the development of two-dimensional mathematical model was motivated.

Kulikovsky et al. [18] developed a vapor-feed two-dimensional DMFC model. Their model based on mass conservation equations for concentrations of species and conservation equations of proton and electron currents, which govern the distributions of electrical potentials of membrane and carbon phases. The model equations are coupled by Butler–Volmer source terms, which describe rates of electrochemical reactions in the anode and cathode catalyst layer. They assumed the cell is isothermal and no pressure gradient caused by external sources across the cell. In the study, they considered an ideal membrane, impermeable for gases and fuel penetration, i.e. methanol crossover can be neglected. This might be a very poor assumption. Generally, in liquid-feed cell, the crossover flux can consume up to 30% methanol. In vapor-feed cell, the crossover is much lower, about 10% of the total methanol. In another paper, Kulikovsky [19] numerically studied a liquid-feed DMFC considering methanol transport through the liquid phase and in hydrophilic pores of the anode backing. However, in both Kulikovsky's publications, the important phenomenon of methanol crossover and convective flow in the anode compartment were ignored. Basically speaking, their models for DMFC are simplified 2-D models.

More recently, Wang and Wang [20] presented a 2-D, two-phase model of liquid-feed DMFC. They extended their previous two-phase PEMFC model [21] to include two-phase flow and transport phenomena in the liquid-feed DMFC. 1-D drift flow model was used to describe methanol flow in anode channel. Thus, Wang's model was actually combined 1-D and 2-D model to the different flow channel in DMFC. Compared with Wang's work, we used 2-D homogenous model to describe fluid flow in anode flow channel, which is more precise.

Although different mathematical models were developed, many electrochemical processes and mechanisms are still difficult to be predicted. For instance, the experimental work has shown that there is a significant effect of increasing the oxygen pressure on the cell performance; however, so far no mathematical model is able to predict this effect.

In this study, a general comprehensive 2-D model is developed for two-phase flow, multi-component transport, and detailed electrochemical reactions presented for a liquid-feed DMFC, including electrodes, channels, and PEM separator. The influence of methanol and water transport, carbon dioxide gas flow, and methanol crossover on cell performance is investigated. The transport and electrochemical processes are analyzed numerically and the effects of the anode feed methanol concentration, temperature, flow rate, and pressure on cell performance are studied in details to illustrate the capabilities of the present model. The two-phase transport in anode and cathode, methanol crossover, as well as their effects on cell performance is explored. This model provides a useful tool for the fundamental understanding of transport and electrochemical phenomena in DMFC and for the optimization of cell design and operating conditions. This model is solved numerically and validated against DMFC experimental performance data.

2. Mathematic modeling

The basic structure of DMFC can be seen in Ref. [22]. The electrochemical reaction at anode electrode is below:

$$\text{Anode: } CH_3OH + H_2O \Rightarrow CO_2 + 6H^+ + 6e^- \quad (1)$$

The protons produced in Eq. (1) are transported via migration to the cathode catalyst layer where they are consumed for oxygen reduction. The corresponding oxygen reduction in the cathode is:

$$\text{Cathode: } 3/2O_2 + 6H^+ \Rightarrow 3H_2O - 6e^- \quad (2)$$

The electrons move to the current collector adjacent to the anode catalyst layer and are transported to the cathode layer through the external circuit.

As a first step towards modeling the two-phase distribution and transport in electrode, it is necessary to invoke simplifying assumptions that are commonly made in the current literature [15,20,21,24]. These are as follows:

(i) Isothermal conditions. Assume the cell temperature is constant and uniform everywhere inside the fuel cell; therefore, the heat generation of electrochemical reaction can be neglected.
(ii) The catalyst layer is treated as an infinitely thin surface of reaction.
(iii) The gas phase is an ideal mixture.
(iv) The gas diffusion electrode is isotropic and homogeneous, and characterized by an effective porosity and permeability.
(v) Butler–Volmer kinetics governs the electrochemical reaction in catalyst layers.
(vi) In practice, methanol is mixed with water in certain proportion. The variation of the liquid density caused by the reaction at the anode is neglected.
(vii) At the cathode side, electrochemical reaction consumes gaseous oxygen and produces water. Although the formation of droplets may not affect the hydrodynamics in the channels the water formation has a significant impact on the diffusion properties of gas diffusion layer. Due to a relatively small fraction of the liquid droplets present in cathode gas channel (i.e., mist flow), the two-phase effect can be neglected therein. Hence only the gas flow is considered as far as hydrodynamics is considered.

2.1. Governing equations for porous media

Continuity:

$$\frac{\partial}{\partial x}(\rho u) + \frac{\partial}{\partial y}(\rho v) = 0 \quad (3)$$

where ρ, ρu and ρv are the mixture parameters

$$\rho u = \rho_l u_l + \rho_g u_g \quad (4)$$

$$\rho v = \rho_l v_l + \rho_g v_g \quad (5)$$

$$\rho = \rho_l s + \rho_g (1 - s) \quad (6)$$

where s is the liquid saturation, it will be defined by Eq. (34).

Momentum conservation:

$$\frac{\partial}{\partial x}(\rho u^2) + \frac{\partial}{\partial y}(\rho uv) = -\frac{\partial p}{\partial x} + \frac{\partial}{\partial x}\left(\mu \frac{\partial u}{\partial x}\right) + \frac{\partial}{\partial y}\left(\mu \frac{\partial u}{\partial y}\right) + S_u \quad (7)$$

$$\frac{\partial}{\partial x}(\rho vu) + \frac{\partial}{\partial y}(\rho v^2) = -\frac{\partial p}{\partial y} + \frac{\partial}{\partial x}\left(\mu \frac{\partial v}{\partial x}\right) + \frac{\partial}{\partial y}\left(\mu \frac{\partial v}{\partial y}\right) + S_v \quad (8)$$

where S_u, S_v are source terms for u and v momentum equations, respectively;

μ is mixture dynamic viscosity, which is [20]:

$$\mu = \frac{\rho}{\frac{\kappa_{rl}}{\nu_l} + \frac{\kappa_{rg}}{\nu_g}} \quad (9)$$

Source terms, S_u and S_v for porous media are:

$$S_u = -\frac{\mu}{K}\varepsilon u + \frac{\varepsilon \mu}{K}\frac{n_d M}{\rho}\frac{I_e}{F} \quad (10)$$

$$S_v = -\frac{\mu}{K}\varepsilon v - \rho g \quad (11)$$

where M is the molecular weight of the membrane pore fluid mixture, which can be expressed as, respectively,

$$M = \sum_k X^k M^k \quad (12)$$

$$n_d = \frac{\sum_k n_d^k M^k}{M} \quad (13)$$

where n_d is the fluid drag coefficient, equal to the drag coefficient of water [23].

Species conservation:

The species conservation equation for the two-phase mixture is [20]:

$$\frac{\partial}{\partial x}(\gamma_\alpha \rho u C^k) + \frac{\partial}{\partial y}(\gamma_\alpha \rho v C^k) = \frac{\partial}{\partial x}\left(\rho D^k \frac{\partial C^k}{\partial x}\right) + \frac{\partial}{\partial y}\left(\rho D^k \frac{\partial^2 C^k}{\partial y^2}\right) + \dot{m}^k \quad (14)$$

This is a general species conservation equation applied to CH_3OH, H_2O, CO_2, and O_2. The left side of Eq. (14) is the convection of the species k, and C^k is the mass fraction of species k

$$C^k = \frac{\rho^k}{\rho} \quad (15)$$

$$\rho C^k = \rho_l C_l^k s + \rho_g C_g^k (1 - s) \quad (16)$$

$$C_l^k = \frac{\rho_l^k}{\rho_l}; \quad C_g^k = \frac{\rho_g^k}{\rho_g} \quad (17)$$

where γ_α is advection correction factor, defined as

$$\gamma_\alpha = \frac{\rho(\lambda_l C_l^k + \lambda_g C_g^k)}{\rho_l s C_l^k + \rho_g (1 - s) C_g^k} \quad (18)$$

where λ_l and λ_g are relative mobilities, defined as

$$\lambda_l = \frac{K_{rl}/v_l}{K_{rl}/v_l + K_{rg}/v_g} \tag{19}$$

$$\lambda_g = 1 - \lambda_l \tag{20}$$

The first term of the right side of Eq. (14) is the diffusion of species k for the mixture. And the effective diffusion coefficient can be expressed as

$$\rho D^k = \rho_l s D^k_{l,\mathrm{eff}} + \rho_g (1-s) D^k_{g,\mathrm{eff}} \tag{21}$$

$$D^k_{l,\mathrm{eff}} = (\varepsilon s)^{t_l} D^k_l \tag{22}$$

$$D^k_{g,\mathrm{eff}} = (\varepsilon(1-s))^{t_g} D^k_g \tag{23}$$

The last term in Eq. (14) stands for the source/sink due to electrochemical reactions. On the anode catalyst layer, there is the methanol oxidation reaction that produces carbon dioxide and the cell current density, I. However, on the cathode, there are two simultaneous electrochemical reactions: oxidation of methanol crossed over through the membrane and oxygen reduction. The oxygen reduction reaction current must provide not only the net cell current density (through the external circuit) but also the parasitic current density (I_p) from methanol crossover, which is $I + I_p$. Therefore, the source/sink term, $\dot{m}^k$, in Eq. (14) can be expressed as:

$$\dot{m}^k = \begin{cases} \frac{M^k}{F}\frac{S^k_{R1}}{n_{R1}} I & \text{anode catalyst layer} \\ \frac{M^k}{F}\left[\frac{S^k_{R1}}{n_{R1}} I_p + \frac{S^k_{R1}}{n_{R2}}(I + I_p)\right] & \text{cathode catalyst layer} \\ 0 & \text{others} \end{cases} \tag{24}$$

The parasitic methanol current density, I_p, caused by oxidation of methanol crossover, can be expressed by the methanol crossover rate [20], j^{MeOH},

$$I_p = -\frac{6F j^{\mathrm{MeOH}}}{M^{\mathrm{MeOH}}} \tag{25}$$

The methanol crossover rate, j^{MeOH}, can be dictated as

$$j^{\mathrm{MeOH}} = \left(\rho_l v_l C^{\mathrm{MeOH}} - \rho_l D^{\mathrm{MeOH}}_{l,\mathrm{eff}} \frac{\partial C^{\mathrm{MeOH}}_l}{\partial x}\right)\Bigg|_{\mathrm{cathode}} \tag{26}$$

The first term on the right side of Eq. (26) describes the mass transfer by convection due to the pressure difference between anode and cathode chambers and electro-osmotic drag. And the second term is the mass transfer by diffusion. It should be noted that since the convection term is a function of methanol concentration, which also implicitly depends on the electro-osmotic drag, and diffusion.

The gas–liquid phase equilibrium:

There are three main components, H_2O, CH_3OH, and CO_2 coexisting in anode side both in porous media and fluid channel. The other intermediates such as OH, HO, CO, CH_2OH, etc. produced in the electrochemical reaction can be neglected due to the amounts are very small and the reaction rates are very fast. In the gas–liquid coexisting system, local thermodynamic equilibrium prevails at the phase interface. Hence, the gas phase can be considered saturated with water and methanol vapor. The mass fraction of saturated water vapor depends on the partial pressure and temperature. It can be determined as

$$C^{\mathrm{H_2O}}_{g,\mathrm{sat}} = \frac{M^{\mathrm{H_2O}} p^{\mathrm{H_2O}}_{\mathrm{sat,T}}}{\rho_g RT} \tag{27}$$

ρ_g is gas mixture density, which is determined by the idea gas equation:

$$\rho_g = \frac{p M_{\mathrm{gas}}}{RT} \tag{28}$$

Similarly, the methanol mass fraction in the gas phase is expressed as

$$C^{\mathrm{MeOH}}_{g,\mathrm{sat}} = \frac{M^{\mathrm{MeOH}} p^{\mathrm{MeOH}}_{\mathrm{sat,T}}}{\rho_g RT} \tag{29}$$

where methanol vapor saturated pressure is simply calculated by applying Henry's law:

$$p^{\mathrm{MeOH}}_{\mathrm{sat,T}} = k^{\mathrm{MeOH}}_H x^{\mathrm{MeOH}}_l \tag{30}$$

where x^{MeOH}_l is the liquid phase methanol molar fraction, and k_H is Henry's law constant, which is a function of temperature as below [25]:

$$k^{\mathrm{MeOH}}_H = 0.096 \exp(0.04511(T - 273)) \tag{31}$$

$$x^{\mathrm{MeOH}}_l \approx \frac{M^{\mathrm{H_2O}}}{M^{\mathrm{MeOH}}} C^{\mathrm{MeOH}}_l \tag{32}$$

After water and methanol partial pressure are calculated, the mass fraction of carbon dioxide in gas phase can be determined:

$$C^{\mathrm{CO_2}}_g = \frac{M^{\mathrm{CO_2}}(p - p^{\mathrm{H_2O}}_{\mathrm{sat,T}} - p^{\mathrm{MeOH}}_{\mathrm{sat,T}})}{\rho_g RT} \tag{33}$$

The mass fraction of carbon dioxide in liquid phase is assumed equal to saturated mass fraction in the liquid mixture, i.e., $C^{\mathrm{CO_2}}_l = C^{\mathrm{CO_2}}_{\mathrm{sat}}$.

Then, the liquid saturation in the porous media can be calculated from:

$$s = \frac{\rho^{\mathrm{CO_2}}_g - C^{\mathrm{CO_2}}_g}{\rho_l(C^{\mathrm{CO_2}}_l - C^{\mathrm{CO_2}}) + \rho_g(C^{\mathrm{CO_2}} - C^{\mathrm{CO_2}}_g)} \tag{34}$$

Note that when $C^{\mathrm{CO_2}} < C^{\mathrm{CO_2}}_{l_{\mathrm{sat}}}$, $s = 1$.

At cathode side, assume the oxygen and nitrogen can not dissolve in the water, due to its very low solubility in water, hence

$$C^{\mathrm{O_2}}_l = 0, \quad C^{\mathrm{N_2}}_l = 0, \quad C^{\mathrm{H_2O}}_l = 1 \tag{35}$$

The vapor condenses when the vapor partial pressure reaches its saturated value corresponding to the operation cell temperature; and the saturation vapor pressure is determined as [26]:

$$\log_{10} p_{\mathrm{sat}} = -2.1794 + 0.02953T - 9.1837 \times 10^{-5} T^2 + 1.4454 \times 10^{-7} T^3 \tag{36}$$

Inside the two-phase zone, assume it is under thermodynamic equilibrium, and thus the mass fraction of water in gas phase is given by their equilibrium value,

$$C_{\mathrm{g}}^{\mathrm{H_2O}} = \frac{M^{\mathrm{H_2O}} p_{\mathrm{sat}}}{M_{\mathrm{gas}} p} \tag{37}$$

Similarly, the liquid saturation in the cathode is therefore expressed as

$$s = \frac{\rho C^{\mathrm{H_2O}} - \rho_{\mathrm{g}} C_{\mathrm{g}}^{\mathrm{H_2O}}}{\rho_{\mathrm{l}} - \rho_{\mathrm{g}} C_{\mathrm{g}}^{\mathrm{H_2O}}} \tag{38}$$

The membrane separator is assumed to be fully hydrated with liquid, thus, $s = 1$.

2.2. Governing equations for fluid channel

In this study, we use homogenous model to describe the fluid flow in anode channel. The study of Triplett et al. [27] showed that the homogeneous model is more accurate for the two-phase flow through microcapillary tubes. Fukano and Kariyasaki [28] also noted that the homogeneous model is valid for two-phase bubbly flow because the tube diameter is smaller than 5.6 mm. Because two-phase flow patterns in the DMFC anode have yet to be established quantitatively, based on the experimental observations, it is reasonable to make a homogeneous flow assumption. Homogenous model provides the simplest technique for analyzing two-phase flows. In this model it is assumed that the two phases are well mixed and therefore travel with the same velocities. Suitable average properties (velocity, temperature, density, and viscosity) are determined and the mixture is treated as a pseudo-fluid that obeys the usual equations of single-phase flow. These governing equations are based on the first principles: the conservations of mass, momentum, energy and mass species. The velocity of each phase is computed using the Navier–Stokes equations. The mixing of non-condensable gases in the water can also be included in the model.

Major assumptions:

- Single phase fluid or two-phase mixture is homogeneous
- Thermal and mechanical equilibrium exist between liquid and vapor flowing together (homogenous equilibrium).
- Flow is under steady state condition.

Governing equations:

Continuity:

$$\frac{\partial}{\partial x}(\rho u) + \frac{\partial}{\partial y}(\rho v) = 0 \tag{39}$$

where ρ, is the mixture density, defined as

$$\rho = \rho_{\mathrm{l}}\alpha + \rho_{\mathrm{g}}(1-\alpha) \tag{40}$$

here α is void fraction which is time-averaged fraction of the cross-sectional area or of the volume which is occupied by the gas phase, expressed as

$$\alpha = \frac{V_{\mathrm{g}}}{V_{\mathrm{g}} + V_{\mathrm{l}}} = \frac{1}{1 + \left(\frac{1-x'}{x'}\frac{\rho_{\mathrm{g}}}{\rho_{\mathrm{l}}}\right)} \tag{41}$$

where V_{g} and V_{l} are the volume of gas phase and liquid phase, respectively. x' is the quality, this is the fraction of the mass flow rate defined as

$$x' = \frac{M_{\mathrm{g}}}{M} \tag{42}$$

Quality is a very important variable in two-phase flow. In this study, it mostly depends on the concentration of carbon dioxide. The value of quality increases with the product generation along the flow direction. It also can be expressed as a function of species concentration as

$$x' = \frac{M_{\mathrm{g}}}{M} = \frac{\rho_{\mathrm{g}}(C_{\mathrm{g}}^{\mathrm{CO_2}} + C_{\mathrm{g}}^{\mathrm{H_2O}} + C_{\mathrm{g}}^{\mathrm{MeOH}})}{\rho_{\mathrm{l}}(C_{\mathrm{l}}^{\mathrm{H_2O}} + C_{\mathrm{l}}^{\mathrm{MeOH}} + C_{\mathrm{l}}^{\mathrm{CO_2}})} \tag{43}$$

Conservation of momentum equations:

$$\frac{\partial}{\partial x}(\rho u^2) + \frac{\partial}{\partial y}(\rho uv) = -\frac{\partial p}{\partial x} + \frac{\partial}{\partial x}\left(\mu\frac{\partial u}{\partial x}\right) + \frac{\partial}{\partial y}\left(\mu\frac{\partial u}{\partial y}\right) \tag{44}$$

$$\frac{\partial}{\partial x}(\rho vu) + \frac{\partial}{\partial y}(\rho v^2) = -\frac{\partial p}{\partial y} + \frac{\partial}{\partial x}\left(\mu\frac{\partial v}{\partial x}\right) + \frac{\partial}{\partial y}\left(\mu\frac{\partial v}{\partial y}\right) \tag{45}$$

where μ is the homogenous viscosity. There are many different ways to define the homogenous viscosity. The correlations which have produced reasonable results were given by Isbin et al. [29], and Dukler et al. [30]. The Isbin equation is used in this study as:

$$\frac{1}{\mu} = \frac{x'}{\mu_{\mathrm{g}}} + \frac{1-x'}{\mu_{\mathrm{l}}} \tag{46}$$

Species conservation:

$$\frac{\partial}{\partial x}(\rho uC^k) + \frac{\partial}{\partial y}(\rho vC^k) = \rho D^k\left(\frac{\partial^2 C^k}{\partial x^2} + \frac{\partial^2 C^k}{\partial y^2}\right) \tag{47}$$

where D^k is mixture diffusivity of species k for liquid and gas, it can be expressed as:

$$\rho D^k = \alpha\rho_{\mathrm{g}} D_{\mathrm{g}} + (1-\alpha)\rho_{\mathrm{l}} D_{\mathrm{l}} \tag{48}$$

It is worth pointing out that in Wang's study [20], they neglected the mass diffusion, and considered only mass convection.

In comparison with the governing equations of porous media and fluid channel, it can be found that they are very similar. Thus, they can be solved through a similar numerical scheme. It's convenient to use a single domain technique to solve these governing equations and complicated inter-boundary conditions can be avoided [31].

2.3. Electrochemical kinetics

The electrochemical reactions of methanol oxidation at the anode and oxygen reduction at the cathode are both

complicated multistage processes, which includes formation of the adsorbate on the catalyst surface, absorption and transformation of intermediates. Under different over-potentials the rate limiting step may be different. The reaction rate also depends on the crystalline structure of the catalyst. Instead of going into details of microscopic modeling of these reactions in this study, we choose to parameterize the reaction rates by standard empirical approximations. Generally, two expressions, relationship or Tafel relationship, are often used to describe these reactions. The latter is simple and was used by Scott [32], Wang [20], Ren [33], etc. In any case, these relations combine electrochemical reaction, fluid flow, and mass transfer altogether. In this study, we use Butler–Volmer expression, as written below:

$$I = i^0_{\mathrm{a,ref}} \frac{C^{\mathrm{MeOH}}}{C^{\mathrm{MeOH}}_{\mathrm{ref}}} \left[\exp\left(\frac{\alpha_a F}{RT}\eta_a\right) - \exp\left(\frac{-\alpha_c F}{RT}\eta_a\right)\right] \tag{49}$$

$$I + I^{\mathrm{MeOH}} = i^0_{\mathrm{c,ref}} \left[\frac{C^{\mathrm{O_2}}}{C^{\mathrm{O_2}}_{\mathrm{ref}}}\right]^{0.5} \left[\exp\left(\frac{\alpha_c F}{RT}\eta_c\right) - \exp\left(\frac{-\alpha_a F}{RT}\eta_c\right)\right] \tag{50}$$

η_a is the anode surface overpotential, which drives MeOH oxidation reaction at the anode, and equals the difference between the potential of the anode catalyst layer and membrane ($\eta_a = \varphi_a - \varphi_m$). And η_c is the cathode surface overpotential, which drives oxygen oxidation reaction (Eq. (2)) and "parasitic" methanol reaction. It equals the difference between membrane and cathode catalyst layer ($\eta_c = \varphi_m - \varphi_c$). I^{MeOH} is the 'parasitic' current density caused by MeOH crossover.

2.4. Potential

One of the main objectives of the model is to calculate the overall cell voltage, which can be written as

$$V_{\mathrm{cell}} = E_{\mathrm{cell}} - \eta_a - \eta_c - \eta_{\mathrm{ohmic}} \tag{51}$$

where E_{cell} is the potential difference between the anode and cathode, at the reference current density i^0, corrected for the thermodynamic effects of temperature and pressure. η_a and η_c are the potential loss of MeOH oxidation at anode and oxygen oxidation at cathode, the potential loss of MeOH crossover is also considered in η_c. The Ohmic overpotential, η_{ohmic}, is calculated for the resistance of the membrane. The appropriate expression for E_{cell} is [14]:

$$E_{\mathrm{cell}} = E^0_{\mathrm{cell}} + \Delta T\left(\frac{\partial E}{\partial T}\right) - \Delta N \frac{RT}{nF} \ln\left(\frac{P_2}{P_1}\right) \tag{52}$$

where E^0_{cell} is the thermodynamic equilibrium potential difference of oxygen reduction and methanol oxidation:

$$E^0_{\mathrm{cell}} = U^{\mathrm{O_2}}_0 - U^{\mathrm{MeOH}}_0 \tag{53}$$

where U is the internal energy.

The temperature effect on the cell potential, $\Delta T\left(\frac{\partial E}{\partial T}\right)$, can be found from thermodynamics relations:

$$\Delta T\left(\frac{\partial E}{\partial T}\right)_{\mathrm{P}} = \Delta T \frac{\Delta S}{nF} \tag{54}$$

The right-hand side of Eq. (54) is the pressure effect on the cell voltage.

The Ohmic potential loss can be expressed as

$$\eta_{\mathrm{ohmic}} = I\frac{t_m}{\sigma_m} \tag{55}$$

The conductivity of the membrane, σ_m, can be calculated with an empirical expression [34]

$$\sigma_m = \sigma^{\mathrm{ref}}_m \exp\left[1268\left(\frac{1}{T_{\mathrm{ref}}} - \frac{1}{T}\right)\right] \tag{56}$$

where σ^{ref}_m is the membrane conductivity at the reference temperature.

2.5. Boundary conditions

Inlet:

At the channel inlet, the velocity, species concentration, and pressure are fixed as

$$u_a = u_{a,\mathrm{in}}, \quad v_a = 0, \quad u_c = u^0_{c,\ \mathrm{in}}, \quad v_c = 0 \tag{57}$$

$$C^{\mathrm{MeOH}} = C^{\mathrm{MeOH}}_{\mathrm{in}}, \quad C^{\mathrm{H_2O}}_a = C^{\mathrm{H_2O}}_{a,\mathrm{in}}, \quad C^{\mathrm{H_2O}}_c = C^{\mathrm{H_2O}}_{c,\mathrm{in}}, \quad C^{\mathrm{CO_2}} = 0 \tag{58}$$

$$p_a = p_{a,\mathrm{in}}, \quad p_c = p_{c,\mathrm{in}} \tag{59}$$

Outlet:

At the channel outlet, the velocity, species concentration, and pressure gradients are assumed equals zero

$$\frac{\partial u}{\partial x} = 0, \quad v = 0, \quad \frac{\partial C^k}{\partial x} = 0, \quad \frac{\partial C^k}{\partial y} = 0, \quad \frac{\partial p}{\partial x} = 0, \quad \frac{\partial p}{\partial y} = 0. \tag{60}$$

Interfaces:

At the surface of anode and cathode collectors, the velocity, species concentration gradients and pressure gradient are set to be zero

$$u = 0, \quad v = 0, \quad \frac{\partial C^k}{\partial y} = 0, \quad \frac{\partial p}{\partial y} = 0 \tag{61}$$

Inner interfaces:

In this study, however, no boundary conditions are required at all inner interfaces, since the governing equations are solved in a "*single domain*".

3. Numerical modeling

3.1. Description of the modeling domain

The basic geometric configuration of the DMFC and the coordinate system is shown in Fig. 1. Basic geometric parameters are summarized in Table 1.

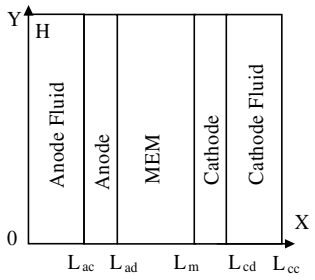

Fig. 1. Physical domain and coordinates.

Table 1
Basic geometric parameters of the DMFC

$\mathbf{L}_{ac}$	2 mm	$\mathbf{L}_{cd}$	0.1 mm	ε_{ad}	0.7	K_{ad}	10^{-11} m
$\mathbf{L}_{ad}$	0.1 mm	$\mathbf{L}_{cc}$	2 mm	ε_{cd}	0.7	K_{cd}	10^{-11} m
$\mathbf{L}_{m}$	0.2 mm	**H**	20 mm	ε_{m}	0.3	K_{m}	10^{-14} m

3.2. The generic conservation equation

It can be seen that the governing equations in porous media and in fluid channel are very similar Eqs. (7), (8), (14), (44) and (45) so that the porous media and fluid channel can be modeled as a single domain. For numerical purposes it is useful to find a generic conservation equation, from which one can obtain the equations of conservation of mass, momentum and mass species in the vapor and in the liquid phase. This generic conservation equation in Cartesian coordinates can be written as

$$\frac{\partial(\rho U\phi)}{\partial x}+\frac{\partial(\rho V\phi)}{\partial y}=\left(\frac{\partial}{\partial x}\left(\Gamma\frac{\partial\phi}{\partial x}\right)+\frac{\partial}{\partial y}\left(\Gamma\frac{\partial\phi}{\partial y}\right)\right)+S_{\phi} \tag{62}$$

where ϕ is a generic property, Γ is the diffusivity for the generic property ϕ and S_{ϕ} is the source term. The advantage of the generic conservation equation is straightforward because one has to deal with only one equation of that form in the numerical code. Note that the pressure gradient is included in the source term just for convenience in the notation. However, this term is treated separately since the pressure field has to be obtained as part of the solution. A pressure correction (or pressure equation) can be derived from the momentum equation to enforce mass conservation. This is the basis of the SIMPLE-like algorithms, such as SIMPEC, SIMPLER and PISO.

In this study a fully implicit method is used. A finite volume method (i.e. SIMPLEC) is used to discretize the governing equations.

3.3. The grid convergence test

Non-uniform mesh sizes of 61×81, 101×121 with a grid variation ratio of 1.1 are used for the grid independence tests. For the grid sizes of 61×81 and 101×121, the changes in predicted species concentration and current density are less than 0.5%. The velocities both in porous media and flow channel are less than 0.1% in the same location with same flow condition. Therefore, grid size of 101×121 is used throughout this study.

4. Results and discussion

4.1. Validation of the present DMFC model

Fig. 2 shows the present DMFC numerical results compared with Scott et al.'s [35] experimental data. Scott et al. [35] performed an experimental study of DMFC. The operating conditions for their experiments are: 0.25 M and 0.5 M solution, cathode exit pressure: 2.0 bar, operation temperature: 60 and 80 °C respectively. In order to compare with their experimental data, an exactly identical operation conditions are selected in this numerical study. Fig. 3 shows that the numerical results agree with the experimental data very well. It can be seen clearly that the operation temperature affects the chemical kinetics. The temperature causes the cell open potential varies significantly. At 60 °C, the open potential is 750 mV; at 80 °C, the open potential is 800 mV. The validation and the following kinetics equation are fitted to the experimental data, which is applied in this validation simulation. How the operation temperature affects the cell performance will be discussed later.

4.2. The effects of methanol concentration on cell performance

Fig. 3 shows the effects of methanol feed concentration on the polarization curves under the following operating conditions, 80 °C, methanol solution flow rate of 2 ml/min, air pressure 1.5 bar, air flow rate 800 ml/min. It can be seen that the methanol concentrations affect the cell polarization curve significantly.

At low current density, e.g., less than 45 mA, high methanol concentration, 2 M and 1.5 M, causes a lower cell voltage and open circuit potential. This is because of the methanol crossover. In this case, methanol molecules cannot be completely consumed to produce current. Some of the methanol molecules must penetrate through the membrane and be oxidized at the cathode side. It causes a mixed potential at the cathode, which is higher with higher concentration of methanol. Thereby, the cell open potential and cell operation potential decrease. For instance, in this study, the open potential is about 730 mV at 1 M, 710 mV at 1.5 M, and 695 mV at 2 M.

At high current density, e.g., more than 150 mA/cm^2, high methanol concentration has better performance. This is because the methanol concentration dominates the cell performance in this region.

For the low methanol concentration, for instance 0.25 M, the polarization curve is mainly dominated by concentration (concentration polarization). The ohmic polarization curve is very short. As the current density increases, the cell potential drops very fast. The current density can-

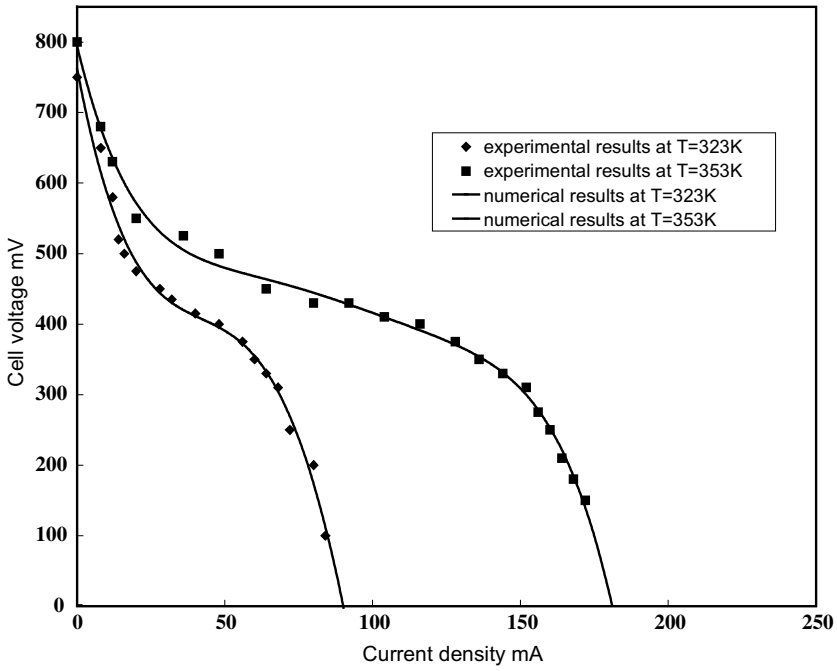

Fig. 2. Polarization curve of the numerical results and experimental data at two different temperatures.

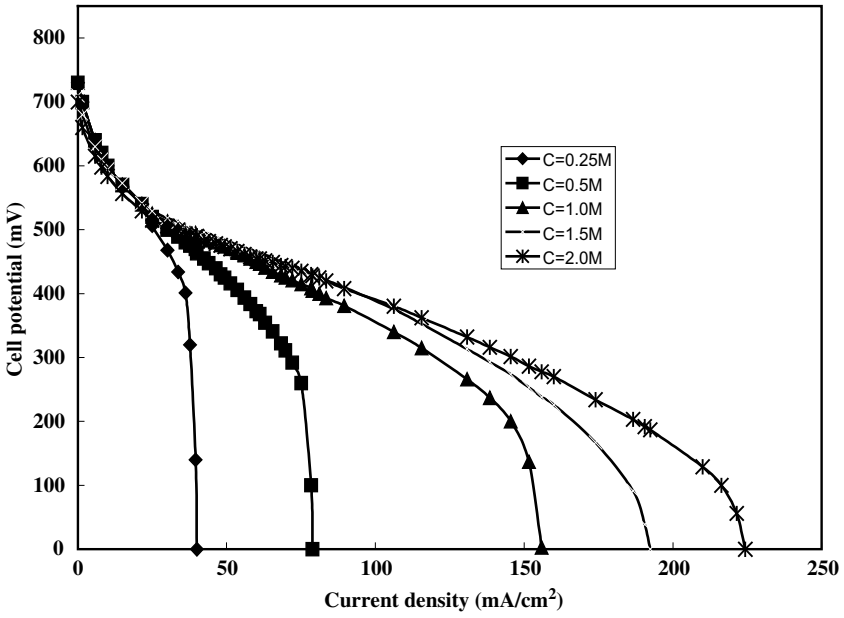

Fig. 3. The effects of methanol concentration on cell performance.

not even reach 50 mA/cm^2. Actually, when the current density increases, more methanol molecules are consumed by the electro-chemical reaction. However, since the methanol concentration is very low; there is not enough methanol molecules that can reach the catalyst layer in time. The mass transfer speed dominates the electron-chemical reaction, further affects the polarization curve. When the methanol concentration increases, the cell performance improves, such as the curve 0.5 M, 1.0 M and 1.5 M, and the ohmic polarization region becomes longer. Usually, most DMFC works on the concentration from 0.5 M to 1.5 M. However, when the methanol concentration is more than 1.5 M, such as 2 M in Fig. 3, somehow, the cell performance does not improve; instead it is worse at the low current density region. This is again because of the methanol crossover. In the high feed methanol concentration, the electron-chemical reaction cannot consume all the methanol molecules on the catalyst layer; the rest of the methanol penetrates through the membrane and directly reaction with the oxygen at the cathode side. This significantly

reduces the oxygen ions creation; further lowers the cell performance and wastes fuel. From Fig. 3, it seems that the high current density can restrict the methanol crossover under operation of the high feed concentration, because high current density consumes more methanol. However, the cell potential is very low. Note that the power output equals cell potential by current density. Thus, the overall power output is pretty low. This is not our expectation.

To conclude, better cell performance is achieved with medium feed concentrations at medium current densities. Operating with small feed concentrations is restricted by low limiting current densities. Operating with high methanol feed concentration suffers from excessive methanol crossover.

4.3. The effects of the temperature on cell performance

Fig. 4 shows the cell polarization curves for 0.25 M methanol solution at the temperature variation from 70 to 95 °C, methanol solution flow rate of 2 ml/min, air pressure at 1.5 bar, and air flow rate at 800 ml/min. It is obviously to see the cell performance significantly enhanced with the temperature increase until 90 °C. The cell voltage and limiting current densities are both high at high temperatures. This result is consistent with experimental conclusion from Scott et al. [35]. It is known that the chemical kinetic energy of the molecules increases with temperature. This means that more protons and ions can be created as seen from Eqs. (1) and (2). Also, it is worth noting that the mass transfer coefficient increases with the temperature. In the range 70–95 °C, the value of diffusion coefficient increases approximately 55%, from 6.08×10^{-8} cm/s to 9.83×10^{-8} cm/s. All these are positive factors to enhance the cell performance.

The cell open circuit potential particularly increases with temperature. The open circuit potential is related to methanol and oxygen internal energy. However, the temperature between 90 and 95 °C on Fig. 4, virtually no additional performance enhancement is seen. This is similar to the result obtained by Baldauf and Preidel [36] between 90 and 100 °C. It is because at the high temperatures, over 90 °C, the methanol and water can easily transfer through the membrane which influences the methanol crossover rate through the membrane. This result indicates that design of a DMFC system for an operating temperature above 90 °C is not likely to be beneficial. The better performance enhancement can be obtained by operating temperature between 60 and 80 °C.

4.4. The effects of the pressure on cell performance

The influence of cathode pressure on cell performance is shown in Fig. 5. The operation condition of this calculation is at methanol concentration 0.5 M and temperature 80 °C. There is a significant effect of increasing the air pressure on the cell performance. The cell voltage increases up to approximately 100 mV as the pressure increase by 1 atm and the limiting current density also significantly increases. This result agrees with Scott's observation in his experimental study [14]. Actually, oxygen volume concentration increases with the pressure increase. As a result, more oxygen molecules per unit volume in the catalyst, creates more oxygen ions create. Thus the electro-chemical reaction rate is speeded up and the methanol crossover greatly reduces. It can be seen the cell open potential also increases with the pressure.

It can be concluded that the increase of cathode pressure is beneficial to cell performance. However, cell operation

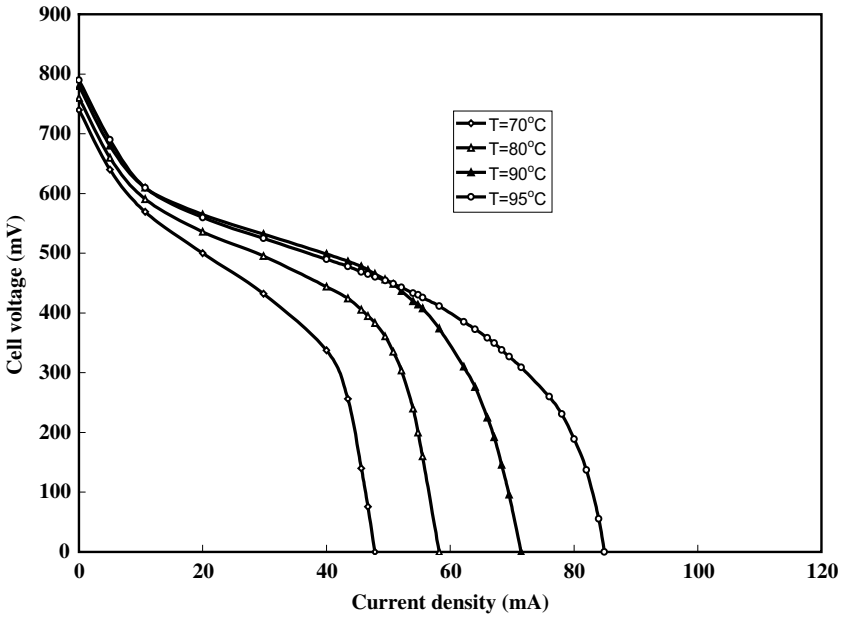

Fig. 4. The polarization curve with different temperature.

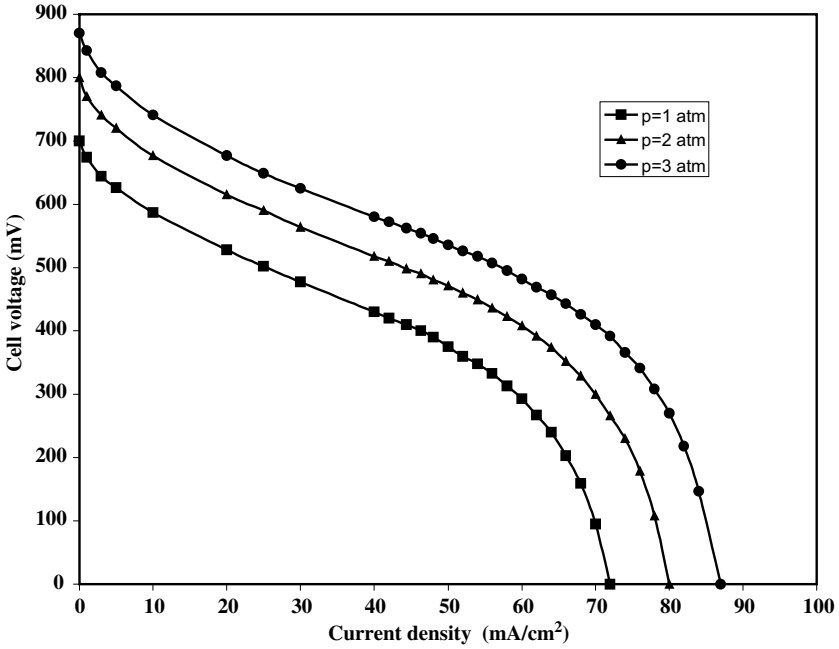

Fig. 5. The effect of pressure on cell performance.

pressure is restricted by the membrane strength. If the cathode pressure is too high the membrane might be damaged. Therefore, it's necessary to optimize the cell pressure.

4.5. The effects of the membrane thickness on cell performance

The thickness of membrane has significant influence on cell performance and methanol crossover. As it was discussed previously, in most of the study, Nafion® membranes are used as solid polymer electrolyte in DMFCs. Currently there are three different thickness of Nafion® membrane developed by DuPont, Nafion® 117, 115 and 112. The thicknesses are 0.18 mm, 0.13 mm and 0.05 mm. In this numerical study, we simulated the cell performance based on these three kinds of membrane at 80 °C. The results are plotted on Fig. 6. The cell has a better performance for thinner membrane. But the open circuit voltage decreases with the reduction of the membrane thickness. As shown on Fig. 6, there are a few crosspoints on the *I–V* curves of the Nafion® 117, 115 and 112. Actually, the thickness of the membrane has two different impacts on cell performance. On one hand, at larger thickness of membrane, the ohmic resistance of the cell is higher. It causes

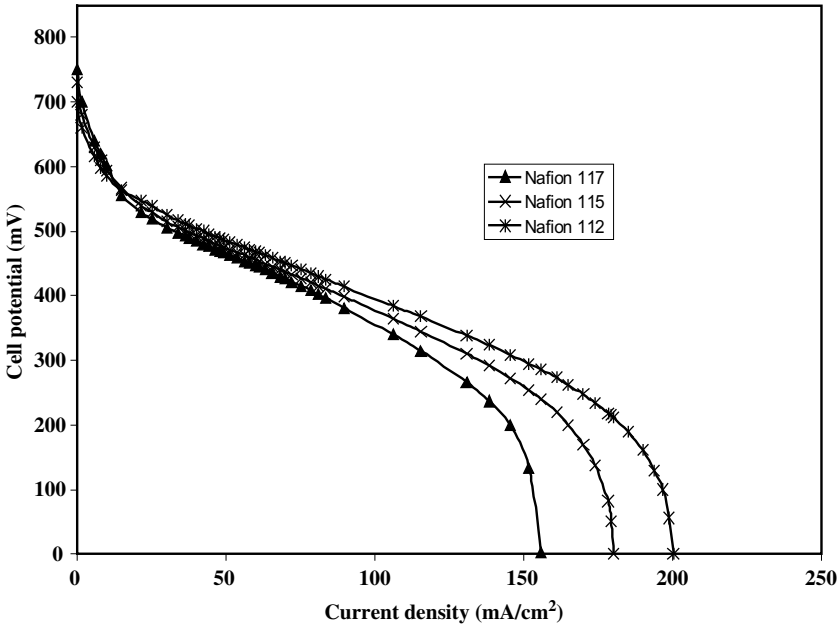

Fig. 6. *I–V* curve on different membrane thickness.

the reduction of ionic conductivity. As a result the cell voltage ohmic loss increases and the power output decreases with the increase in membrane thickness. On the other hand, methanol crossover decreases when the thickness of the membrane increases because the mass transfer resistance in the membrane increases. As a result, the electrical performance of DMFC with membranes of various thicknesses is determined by the combined effects of ionic conductivity and fuel crossover. This result agrees with the experimental observation by Narayanan et al. [37,38] and Jung et al. [39].

4.6. The effects of the flow rate on cell performance

Fig. 7 shows the influence of the variation of the methanol solution flow rate in the range of 5–9 ml/min at 0.5 M and at a temperature of 80 °C. The influence of the methanol flow rate on the limiting current density behaviors is quite complicated. As shown on Fig. 7, the cell voltages at fixed current densities increase with methanol flow rates (from 5 ml/min to 7 ml/min). But as flow rates exceeds 7 ml/min, such as 8 ml/min and 9 ml/min, the cell performance decreases. Actually, flow rate influences the limiting current density or polarization characteristics through convection of methanol solution, i.e. methanol concentration in the cell. Scott et al. [40] introduced Damkoehler number to investigate the influence of methanol convection on the mass transfer. It was defined as: $Da = \frac{1}{QC_o}\left(\frac{iA_{cell}}{6F}\right)$.

At low Damkoehler number of 0.2–0.5, mass transfer coefficient increases with *Da* increase, indicating a beneficial effect of increase in flow rate as shown in Fig. 7, 5 ml/min, 6 ml/min and 7 ml/min. At high *Da* number, more than 0.5, the mass transfer coefficient decrease with *Da* increase, which means mass transfer coefficient decreases with the flow rate increases, as seen on Fig. 7 for the curves of 8 ml/min and 9 ml/min.

5. Concluding remarks

A two-dimensional (2D) two-phase flow model with mixed potential effects has been developed for the liquid-feed DMFC. In comparison to the existing two-phase flow model for DMFC, this model has significantly improved the theoretical DMFC model in the following aspects:

- The macroscopic velocity field in the porous media is provided by expressions obtained by the volume-averaged Navier–Stokes equations combined with a generalized form of Darcy's law. Velocity diffusion terms, pressure gradients, gravity, and electro-osmotic drag are taken into consideration in the momentum equations. To include all these effects, a much more complex governing equations are solved. These has not been done in any of the previous 2D DMFC models.
- Electrochemical kinetics was described by Bulter–Volmer correlations, instead of Tafel correlation. Note that Bulter–Volmer correlations have better performance even at lower current densities.
- The effects of both pressure and temperature for the potential difference between the anode and cathode are considered in this study.
- The governing equations are solved in a single domain, which eliminates the need for assumptions in the complex inner interface boundaries.

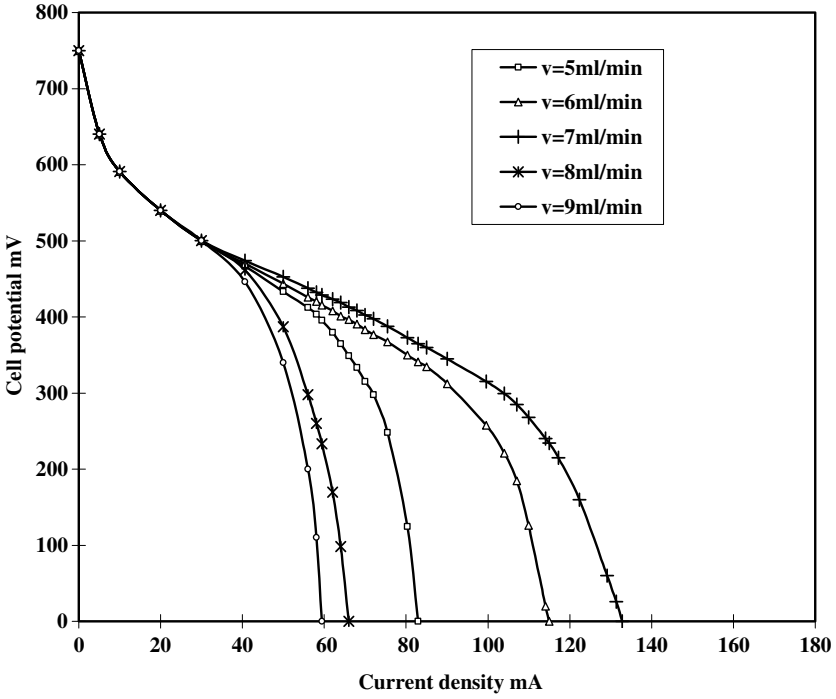

Fig. 7. The effects of the flow rates on cell performance.

This two-dimensional, two-phase flow model was solved numerically. The numerical results agree well with published experimental data. The impacts of the methanol concentration flow rate, cell operation current density, and cell temperature on direct methanol fuel cell performance have been discussed in details.

Acknowledgements

The authors thank the National Science Foundation (through NSF-GOALI DMII-9908324), and UW System Applied Research Award for their financial support of the Project.

References

[1] A.K. Sukla, M.K. Ravikumar, K.S. Gandhi, Direct methanol fuel cells for vehicular applications, J. Solid State Electrochem. 2 (1998) 117.
[2] K. Scott, W. Taama, J. Cruickshank, Performance of a direct methanol fuel cell, J. Appl. Electrochem. 28 (1998) 289.
[3] W.F. Lin, J.T. Wang, R.F. Savinell, On-line FTIR spectroscopic investigations of methanol oxidation in a direct methanol fuel cell, J. Electrochem. Soc. 144 (1997) 1917.
[4] S.J.C. Cleghorn, X. Ren, T.E. Springer, M.S. Wilson, C. Zawodzinski, T.A. Zawodzinski, S. Gottesfeld, PEM fuel cells for transportation and stationary power generation applications, Int. J. Hydrogen Energy 22 (1997) 1137.
[5] B. Guran, R. Viswanathan, R.X. Liu, T.J. Lafrenz, K.L. Ley, E.S. Smotkin, E. Reddington, A. Sapienza, B.C. Chan, T.E. Mallouk, S. Sarangapani, Structural and electrochemical characterization of binary, ternary, and quaternary platinum alloy catalysts for methanol electro-oxidation, J. Phys. Chem., B 102 (1998) 9997.
[6] M. Watanabe, M. Uchida, S. Motoo, Preparation of highly dispersed Pt + Ru alloy clusters and the activity for the electrooxidation, J. Electroanal. Chem. 229 (1987) 395.
[7] A. Hamnett, Mechanism and electrocatalysis in the direct methanol fuel cell, Catal. Today 38 (1997) 445.
[8] N.M. Markovic, H.A. Gasteiger, P.N. Ross, X.D. Jiang, I. Villegas, M.J. Weaver, Electrooxidation mechanisms of methanol and formic acid on Pt–Ru alloy surfaces, Electrochim. Acta 40 (1995) 91.
[9] S.C. Thomas, X. Ren, S. Gottesfeld, Influence of ionomer content in catalyst layers on direct methanol fuel cell performance, J. Electrochem. Soc. 146 (1999) 4354.
[10] S. Arico, P. Creti, E. Modica, G. Monforte, V. Baglio, V. Antonucci, Investigation of direct methanol fuel cells based on unsupported Pt–Ru anode catalysts with different chemical properties, Electrochim. Acta 45 (2000) 4319.
[11] M.K. Ravikumar, A.K. Shukla, Effect of methanol crossover in a liquid-feed polymer-electrolyte direct methanol fuel cell, J. Electrochem. Soc. 143 (1996) 2601.
[12] Narayanan, S.R., Frank, H., Jeffries-Nakamura, B., Smart, M., Chun, W., Halpert, G., Kosek, J., Cropley, C., 1995. In: Gottesfeld, S., Halpert, G., Landgrebe, A. (Eds.), Proton Conducting Membrane Fuel Cells I, The Electrochemical Society Proceedings Series, Pennington, NJ.
[13] M.W. Verbrugge, Methanol diffusion in perfluorinated ion-exchange membranes, J. Electrochem. Soc. 136 (1989) 417–423.
[14] K. Scott, W. Tamma, J. Cruickshank, Performance and modeling of a direct methanol solid polymer electrolyte fuel cell, J. Power Source 65 (1997) 159.
[15] S.F. Baxter, V.S. Battaglia, R.E. White, Methanol fuel cell model: anode, J. Electrochem. Soc. 146 (2000) 437.
[16] Wang, J.T., Savinell, R.F., 1994. In: Srinivasan, S., Macdonald, D.D., Khandkar A.C. (Eds.), Electrode Materials and Processes for Energy Conversion and Storage, PV 94-23, The Electrochemical Society Proceedings Series, Pennington, NJ, p. 326.
[17] H. Dohle, J. Divisek, R. Jung, Process engineering of the direct methanol fuel cell, J. Power Sources 86 (2000) 469.
[18] A. Kulikovsky, J. Divisek, A.A. Kornyshev, Two-dimensional simulation of direct methanol fuel cells, a new type of current collector, J. Electrochem. Soc. 147 (2000) 953.
[19] A.A. Kulikovsky, Two-dimensional numerical modelling of a direct methanol fuel cell, J. Appl. Electrochem. 30 (2000) 1005.
[20] Z.H. Wang, C.Y. Wang, Mathematical modeling of liquid-feed direct methanol fuel cells, J. Electrochem. Soc. 150 (4) (2003) 508–519.
[21] Z.H. Wang, C.Y. Wang, K.S. Chen, Two-phase flow and transport in the air cathode of proton exchange membrane fuel cells, J. Power Sources 94 (2001) 40–50.
[22] Kai Sundmacher, Keith Scott, Direct methanol polymer electrolyte fuel cell: Analysis of charge and mass transfer in the vapor–liquid–solid system, Chem. Engng. Sci. 54 (1999) 2927–2936.
[23] X. Ren, T.E. Springer, T.A. Zawodzinski, S. Gottesfeld, Methanol transport through nation membranes. Electro-osmotic drag effects on potential step measurements, J. Electrochem. Soc. 147 (2000) 466.
[24] M. Kaviany, Principles of Heat Transfer in Porous Media, Springer, New York, 1995.
[25] M.C. Leverett, Capillary behavior in porous solid, Trans. AIME 142 (1941) 152–169.
[26] M.L. McGlashan, A.G. Williamson, Isothermal liquid–vapor equilibria for system methanol–water, J. Chem. Engng. Data 21 (1976) 196.
[27] K.A. Triplett, S.M. Ghiaasiaan, S.I. Abdel-Khalik, A. LeMouel, B.N. Mc- Cord, Gas–liquid two-phase flow in microchannels, Part II: Void fraction and pressure drop, Int. J. Multiphase Flow 25 (1999) 395.
[28] T. Fukano, A. Kariyasaki, Characteristics of gas–liquid two-phase flow in a capillary tube, Nucl. Engng. Des 141 (1993) 59.
[29] Isbin, H.S., Moen, R.H., Wickey, R.O., Mosher, D.R., Larson, H.C., 1958. In: Two-phase Steam Water Pressure Drops, Nuclear Science and Engineering, Conference, Chicago.
[30] A.E. Dukler, M. Wicks, R.G. Cleveland, Frictional pressure drops in two-phase flow, AIChE J. 10 (1964) 44.
[31] T.C. Jen, T. Yan, S.-H. Chan, Chemical reaction transport phenomena in a PEM fuel cell, Int. J. Heat Mass Transfer 46 (2003) 4157–4168.
[32] K. Scott, W.M. Taama, S. Kramer, P. Argyropoulos, K. Sundmacher, Limiting current behavior of the direct methanol fuel cell, Electrochim. Acta 45 (1999) 945–957.
[33] X. Ren, P. Zelenay, S. Thomas, J. Davey, S. Gottesfeld, Recent advances in direct methanol fuel cells at Los Alamos National Laboratory, J. Power Sources 86 (2000) 111.
[34] T.V. Nguyen, R.E. White, A water and heat management model for proton-exchange-membrane fuel cells, J. Electrochem. Soc. 140 (1993) 2178.
[35] K. Scott, W.M. Taama, P. Argyropoulos, K. Sundmacher, The impact of mass transfer and methanol crossover on the direct methanol fuel cell, J. Power Source 83 (1999) 204–216.
[36] M. Baldauf, W. Preidel, Status of the development of a direct methanol fuel cell, J. Power Sources 84 (1999) 161–166.
[37] S.R. Narayanan, A. Kindler, B. Jeffries-Nakamura, W. Chun, H. Frank, M. Smart, T.I. Valdez, S. Surampudi, G. Halpert, Recent advances in PEM liquid-feed direct methanol fuel cell, Annu. Battery Conf. Appl. Adv. 11 (1996) 113.
[38] S. Suranpudi, S.R. Narayanan, E. Vamos, H. Frank, G. Halpert, A. Laconti, J. Kosek, G.K. Surya Prakash, G.A. Olah, Advances in direct oxidation methanol fuel cells, J. Power Sources 47 (1994) 377–385.
[39] D.H. Jung, C.H. Lee, C.S. Kim, D.R. Shin, Performance of a direct methanol polymer electrolyte fuel cell, J. Power Sources 71 (1998) 169–173.
[40] K. Scott, P. Argyropoulos, K. Sundmacher, A model for the liquid feed direct methanol fuel cell, J. Electroanal. Chem. 477 (1999) 97–110.